Pergamon

Int. J. Heat Mass Transfer. Vol. 38, No. 14, pp. 2657–2666, 1995

0017-9310/95 $9.50 + 0.00

0017-9310(95)00009-7

A nonlinear low-Reynolds-number k–ε model for turbulent separated and reattaching flows—I. Flow field computations

TAE SEON PARK and HYUNG JIN SUNG†

Department of Mechanical Engineering, Korea Advanced Institute of Science and Technology, Taejon, Korea

(*Received* 9 *June* 1994 *and in final form* 13 *October* 1994)

Abstract—An improved version of nonlinear low-Reynolds-number k–ε model is developed. In this model, the limiting near-wall behavior and nonlinear Reynolds stress representations are incorporated. Emphasis is placed on the adoption of R_y ($\equiv k^{1/2}y/\nu$) instead of y^+ ($\equiv u_\tau y/\nu$) in the low-Reynolds-number model for predicting turbulent separated and reattaching flows. The non-equilibrium effect is examined to describe recirculating flows away from the wall. The present model is validated by doing the benchmark problem of turbulent flow behind a backward-facing step. The predictions of the present model are cross-checked with the existing measurements and DNS data. The model performance is shown to be generally satisfactory.

1. INTRODUCTION

Separated and reattaching flows occur in a host of practical engineering situations. Examples may be found in the neighborhood of airfoils, turbine blades, diffusers, and many flow-relevant systems. The flow separation and subsequent reattachment process generates extremely complex flow and heat transfer characteristics, among others, the separated flow, which then reattaches in the downstream locations, is believed to give rise to flow unsteadiness, pressure fluctuations, noise, etc. Also, flow separation tends to enhance heat and mass transfer and augment mixing. Comprehensive knowledge of flow structure is an essential building block to analyze the attendant transport phenomena. This research program represents a multi-prong attack on the problem of turbulent flow and heat transfer processes in separated and reattaching flows [1–3]. In this paper, emphasis is placed on flow structure. In the subsequent papers, detailed discussions will be given on the heat transfer characteristics.

Among the various turbulence models to calculate separated and reattaching flows, the k–ε turbulence model is widely used owing to its simplicity and effectiveness rather than more sophisticated higher-order models [1–5]. However, conventional k–ε models are known to suffer from some deficiencies. One major deficiency of the standard k–ε model is that the effects of wall-proximity are not well reflected in the separated and reattaching regions. A variety of low-Reynolds-number versions of the k–ε model have been proposed by introducing the damping functions and other extra terms to account for the near-wall effects. However, most of the existing models contain the wall friction velocity u_τ [4]. If these u_τ-dependent models are applied to separated and reattaching flows, difficulty arises at the separation and reattachment points ($u_\tau = 0$). Obviously in these regions the wall shear stress cannot be clearly defined and the law of the wall is no longer applicable. Furthermore, the turbulent structure with high turbulence levels in separated and reattaching regions is different from that in a turbulent boundary layer which is determined based on local equilibrium arguments. In the present study, a new low-Reynolds-number version without the usage of u_τ is proposed with the aid of direct numerical simulation (DNS) data [6]. Attention is given to a possible improvement of the near-wall behavior of the ε equation. The present model results for separated and reattaching flows are shown to be in satisfactory agreement with the recent data [7]. It is notable that Abe *et al.* [8] used the Kolmogorov velocity scale instead of u_τ to deal with the near-wall behavior of separated and reattaching flows.

In addition to the consideration of above-mentioned near-wall effect, the effect of non-equilibrium away from the wall is also taken into account in the present model. In the recirculating region, it is known that the production of turbulent energy P_k is not balanced with its dissipation rate ε, i.e. $P_k/\varepsilon \neq 1$ [2, 9]. In order to address this point in the present study, the non-equilibrium effect (P_k/ε) is incorporated in the wall damping function (f_μ) and in the anisotropic production of ε in the near-wall region ($C_{\varepsilon 1}$).

Another significant deficiency in the standard k–ε models is the inability to properly account for streamline curvature, rotational strains, and other body-

†Author to whom correspondence should be addressed.

NOMENCLATURE

C_f mean skin friction coefficient, $2\tau_w/(\rho U_0^2)$
C_μ, $C_{\varepsilon 1}$, $C_{\varepsilon 2}$ model constants of standard k–ε model
$C_{\varepsilon 1}^*$ model constant of additional production of dissipation, $C_{\varepsilon 1}(0.95+0.05P_k/\varepsilon)$
C_o free stream specific heat
D channel width upstream of backward-facing step
ER expansion ratio of backward-facing step, (H+D)/D
f_μ, f_1, f_2, f_t model functions of low-Reynolds-number k–ε model
$f_{\mu 1}$ damping function in wall-affected region
$f_{\mu 2}$ correction of non-equilibrium eddy viscosity away from the wall
f_{w1}, f_{w2} wall-reflection functions
h heat transfer coefficient, $\dot{q}_w''/(T_w - T_o)$
H height of backward-facing step
k turbulent kinetic energy
P_k production of turbulent energy
Pr, Pr_t molecular and turbulent Prandtl number
$\dot{q}_w''$ wall heat transfer rate per unit area
Re_H Reynolds number based on step height, $U_o H/\nu$
Re_m Reynolds number based on channel bulk velocity, $2U_m\delta/\nu$
Re_θ Reynolds number based on momentum thickness, $U_o\theta/\nu$
Re_τ Reynolds number based on friction velocity, $u_\tau\delta/\nu$
R_t turbulent Reynolds number, $k^2/\nu\varepsilon$
R_y nondimensional length from wall surface, $k^{1/2}y/\nu$
S mean strain rate, $\sqrt{2S_{ij}S_{ij}}$
St Stanton number, $h/U_o\rho_o C_o$
T_o free stream temperature
T_w local wall temperature
$-\overline{u_i u_j}$ Reynolds stresses
U_i mean velocity
u_τ friction velocity, $\sqrt{(\tau_w/\rho)}$
u_ε Kolmogorov velocity scale, $(\nu\varepsilon)^{1/4}$
X_R reattachment length
x Cartesian coordinate in streamwise direction
y Cartesian coordinate normal to streamwise direction
y^+ nondimensional length from wall, $u_\tau y/\nu$.

Greek symbols
δ half width of channel
δ_{ij} Kronecker delta
ε dissipation rate of turbulent energy, $\overline{\nu(\partial u_i/\partial x_j)(\partial u_i/\partial x_j)}$
ν, ν_t kinematic viscosity and eddy viscosity
ρ density
σ_k, σ_ε model constants in turbulent diffusion of k–ε model
τ_w wall shear stress.

Subscripts
0 reference value at inlet to backward-facing step.

force effects. In the k–ε models, the principal axes of the stress tensor are aligned with those of the mean strain rate tensor. However, in complex turbulent recirculating region, these axes are not always coincident with each other. In order to consider these effects, a nonlinear k–ε model is applied in the present study. A literature survey reveals that a considerable research effort has been directed toward the development of nonlinear or anisotropic generalization of eddy-viscosity models [10]. The present model adopts the Reynolds stresses up to the second-order expansion. The implementation procedure of the model will be recapitulated in the following sections.

In summary, we propose an improved version of nonlinear low-Reynolds-number k–ε model, in which the near-wall effect of separated and reattaching flows and the nonlinear representation for Reynolds stresses are fully incorporated. Emphasis is placed on the usage of R_y ($\equiv k^{1/2}y/\nu$), instead of y^+ ($\equiv yu_\tau/\nu$), in the low-Reynolds-number model, together with the wall limiting behavior of the ε-equation. The non-equilibrium effect is taken into account to deal with the complex recirculation region for separated and reattaching flows away from the wall. In particular, the nonlinear model up to second-order expansion considering the effect of near-wall behavior is also examined. The validation of the improved version is then applied to the turbulent flow behind a backward-facing step, which is frequently used for benchmarking the performance of turbulence models for separated and reattaching flows. If a turbulence model can reproduce this flow correctly, then the possibilities that the model is equally successful with other types of turbulent flow would be high. As mentioned earlier, the accurate prediction of heat transfer in separated and reattaching flows is impossible without reliable predictions of the flow [8]. The predicted results of the present model are compared and evaluated with the relevant measurements [11–14] and computation [8], especially with the DNS data of a backward-facing

step flow [7]. Furthermore, comparisons are extended to the heat transfer in a backward-facing step flow [15].

2. LOW-REYNOLDS-NUMBER k–ε MODEL

2.1. *Governing equations*

For a stationary, incompressible turbulent flow, the governing equations can be written in Cartesian tensor notation as

$$\frac{\partial U_i}{\partial x_i} = 0 \tag{1}$$

$$U_j \frac{\partial U_i}{\partial x_j} = -\frac{1}{\rho}\frac{\partial P}{\partial x_i} + \frac{\partial}{\partial x_j}\left[\nu \frac{\partial U_i}{\partial x_j} - \overline{u_i u_j}\right] \tag{2}$$

where U_j and u_j are the jth components of the mean and fluctuating velocities, respectively, P is the mean pressure, ρ and ν are the fluid density and kinematic viscosity. The unknown Reynolds stress $-\overline{u_i u_j}$ can be expressed, by using the concept of eddy viscosity ν_t:

$$\begin{aligned} -\overline{u_i u_j} = {} & 2\nu_t S_{ij} - \tfrac{2}{3}k\delta_{ij} \\ & + C_1 \nu_t \frac{k}{\varepsilon}(S_{im}S_{mj} - \tfrac{1}{3}S_{mn}S_{mn}\delta_{ij}) \\ & + C_2 \nu_t \frac{k}{\varepsilon}(\omega_{im}S_{mj} + \omega_{jm}S_{mi}) \\ & + C_3 \nu_t \frac{k}{\varepsilon}(\omega_{im}\omega_{jm} - \tfrac{1}{3}\omega_{mn}\omega_{mn}\delta_{ij}) \end{aligned} \tag{3}$$

$$\nu_t = C_\mu f_\mu \frac{k^2}{\varepsilon} \tag{4}$$

$$U_j \frac{\partial k}{\partial x_j} = \frac{\partial}{\partial x_j}\left[\left(\nu + f_t \frac{\nu_t}{\sigma_k}\right)\frac{\partial k}{\partial x_j}\right] + P_k - \varepsilon \tag{5}$$

$$\begin{aligned} U_j \frac{\partial \varepsilon}{\partial x_j} = {} & \frac{\partial}{\partial x_j}\left[\left(\nu + f_\varepsilon \frac{\nu_t}{\sigma_\varepsilon}\right)\frac{\partial \varepsilon}{\partial x_j}\right] \\ & + P_\varepsilon^1 + P_\varepsilon^2 + P_\varepsilon^3 + P_\varepsilon^4 - \gamma. \end{aligned} \tag{6}$$

In the above equations, $-\overline{u_i u_j}$ is expanded up to the second-order term in a nonlinear k–ε model [10], where

$$S_{ij} = 0.5(U_{i,j} + U_{j,i}) \quad \omega_{ij} = 0.5(U_{i,j} - U_{j,i}) \tag{7}$$

are the mean strain rate tensor and mean vorticity tensor, respectively. C_1, C_2, C_3, C_μ, σ_k and σ_ε are the model constants. f_t represents the model function for turbulent diffusion. The f_μ function reflects the effects of wall-proximity and low-Reynolds-diffusion. The f_μ function reflects the effects of wall-proximity and low-Reynolds-number, respectively. The production of turbulent energy, P_k is defined as $P_k \equiv -\overline{u_i u_j}\,\partial U_i/\partial x_j$. In the ε-equation, $P_\varepsilon^1, P_\varepsilon^2, P_\varepsilon^3, P_\varepsilon^4$ and γ represent the mixed production, production by mean velocity gradient, gradient production, turbulent production and destruction in sequence, respectively [6].

2.2. *Model functions* f_μ *and* f_t

In the near-wall region, the asymptotic behavior of instantaneous velocity components maintains the relations $u \propto y$, $v \propto y^2$ and $w \propto y$, and $\varepsilon = \nu\overline{(\partial u_i/\partial x_j)(\partial u_i/\partial x_j)} \to \varepsilon_w$ for $y \to 0$. Consequently, the near-wall asymptotic behavior of wall turbulence is $k \propto y^2$, $\overline{uv} \propto y^3$ and $\nu_t \propto y^3$. Then, the damping function f_μ has to satisfy the relation, $f_\mu \propto y^{-1}$ [5]. The appropriate modeling of ν_t from the buffer to log-law region is critical to the prediction of mean flow field. Most of f_μ functions in the literature are constructed by using the friction velocity u_τ [4]. As emphasized in the introduction, if we applied these models to separated and reattaching flows, difficulties are encountered at a separation point ($u_\tau = 0$) and at a reattaching location ($u_\tau = 0$). Instead of $y^+ (= u_\tau y/\nu)$ in the f_μ model function, the length scale variable R_y is employed in the present study, which is defined by $R_y = k^{1/2}y/\nu$. It is noted that the R_y function was already used in other models, e.g. Lam and Bremhorst [16] and Zhang and Sousa [17]. However, these previous models fail to satisfy the wall-limiting behavior, i.e. $f_\mu \propto y^{-1}$. The usage of R_y instead of y^+ implies that the friction velocity u_τ is replaced by $k^{1/2}$ to account for separated and reattaching flows.

The form similar to the Van Driest damping function has been used in many previous models for representing the wall-proximity effects [4], in which the model constant C_μ is set to be constant, $C_\mu = 0.09$. When f_μ is introduced to predict the damping of eddy-viscosity near the wall, then f_μ must approach 1 far away from the wall, which indicates that the standard k–ε model form is recovered. However, the local equilibrium ($P_k = \varepsilon$) is no longer satisfied in the recirculating region away from the wall. In order to incorporate the non-equilibrium effect ($P_k \neq \varepsilon$), variations of C_μ are allowed in the present study, i.e. $f_\mu = f_{\mu 1} f_{\mu 2}$. By using this expression, it is intended that f_μ takes into account the two major dynamic effects; $f_{\mu 1}$ signifies the effect of wall proximity in the near-wall region and $f_{\mu 2}$ represents the effect of non-equilibrium away from the wall.

In the first, the distribution of eddy-viscosity, $f_{\mu 1}$, near the wall ($C_\mu = 0.09$) can generally be obtained by introducing the Van Driest damping function [4],

$$f_{\mu 1} = (1 - f_{w1})(1 + 10 f_{w1}/R_t^{1.25}) \tag{8}$$

$$f_{w1} = \exp[-(R_y/80)^2] \tag{9}$$

where R_t denotes the turbulent Reynolds number, $R_t = k^2/\nu\varepsilon$. The wall-reflection function f_{w1} represents the effect of wall-proximity. Obviously, $f_{\mu 1}$ satisfies the limiting behavior $f_{\mu 1} \propto y^{-1}$.

Next, it is known that C_μ varies as a function of P_k/ε, away from the wall ($f_{\mu 1} = 1$), as demonstrated in the experimental findings of Rodi [9]. In order to formulate the C_μ form in the non-equilibrium region, the following relation is derived from the algebraic stress model for an attached two-dimensional flow [9],

$$-\overline{uv} = \frac{2}{3}\frac{(1-C_2)(C_1-1+C_2P_k/\varepsilon)}{(C_1-1+P_k/\varepsilon)^2}\frac{k^2}{\varepsilon}\frac{\partial U}{\partial y} = C_\mu f_{\mu 2}\frac{k^2}{\varepsilon}\frac{\partial U}{\partial y} \quad (10)$$

where C_1 and C_2 are the model constants. From the above relation, the model function $f_{\mu 2}$ can be formulated, which accounts for the non-equilibrium effect away from the wall. A simplified function $f_{\mu 2}$ is proposed in the present study,

$$f_{\mu 2} = C_{\mu 1}\frac{(C_{\mu 2}+C_{\mu 3}P_k/\varepsilon)}{(C_{\mu 2}+P_k/\varepsilon)^2} \quad (11)$$

where the model constants are fitted by using the experimental data [9] as $C_{\mu 1} = 2.62$, $C_{\mu 2} = 1.2$ and $C_{\mu 3} = 0.646$, respectively. In summary, the damping function is expressed as $f_\mu = f_{\mu 1}f_{\mu 2}$, where $f_{\mu 1}$ varies mainly with the variable R_y in the wall-affected region, while the variation of $f_{\mu 2}$ plays a leading role for the correction of non-equilibrium eddy-viscosity away from the wall.

The turbulent diffusion terms of k and ε, in general, modeled by a gradient-diffusion type. The values of the model constants σ_k and σ_ε are usually taken to be $1.0 \leqslant \sigma_k, \sigma_\varepsilon \leqslant 1.4$, as shown in [4]. However, as seen in the budgets of k and ε from the DNS data [6], the roles of turbulent diffusion in the near-wall region are substantial. Accordingly, a modified model function f_t is needed, and this concept has been embedded in the model of Nagano and Shimada [18]. The model constants employed are, as denoted in equations (5) and (6), $\sigma_k = 1.2$, $\sigma_\varepsilon = 1.3$ and $f_t = 1+3.5\exp[-(R_t/150)^2]$. This relation implies that the model constants σ_k and σ_ε are adjusted as a function of turbulent Reynolds number R_t in the near-wall region.

2.3. *Near-wall modeling of ε-equation*

According to the order-of-magnitude analysis in the ε-equation, the dominant elements are the turbulent production rate P_ε^4 due to vortex stretching and the viscous destruction γ in the high-Reynolds-number region away from the wall [19]. On the contrary, the production terms P_ε^1 and P_ε^2 become increasingly important near the wall. In order to balance the ε-budget, these effects should be incorporated in the turbulence models. By following the scaling argument of Rodi and Mansour [19], the magnitude of the production terms P_ε^1 and P_ε^2 relative to the terms $P_\varepsilon^4-\gamma$ may be estimated to be

$$\frac{P_\varepsilon^1-P_\varepsilon^2}{P_\varepsilon^4-\gamma} = O\left(\frac{Sk}{\varepsilon}\frac{1}{R_t^{1/2}}\right) = O(R) \quad (12)$$

where S represents the magnitude of strain rate, $S = \sqrt{(2S_{ij}S_{ij})}$ and R is the ratio of the timescale of dissipative motions to the timescale of mean strain fields. Based on this reasoning, the $P_\varepsilon^1, P_\varepsilon^2, P_\varepsilon^4$ and γ terms can be modeled in a way similar to the prior models [4, 5, 18],

$$P_\varepsilon^1+P_\varepsilon^2+P_\varepsilon^4-\gamma = C_{\varepsilon 1}^* P_k\frac{\varepsilon}{k}-C_{\varepsilon 2}f_2\frac{\varepsilon^2}{k}. \quad (13)$$

Here, the model constant $C_{\varepsilon 1}^*$ has the form, $C_{\varepsilon 1}^* = C_{\varepsilon 1}(0.95+0.05P_k/\varepsilon)$. Clearly, in the present model, the non-equilibrium relation (P_k/ε) is properly taken into consideration, and this aspect takes care of the additional production of dissipation by local anisotropy. However, the model constants $C_{\varepsilon 1}$ and $C_{\varepsilon 2}$ are set to take the standard values of 1.45 and 1.9, respectively.

The model function f_2, which deals with the sum of source and sink terms in the near-wall region, is defined as,

$$f_2 = (1+f_{21})(1-f_{w2})f_{22} \quad (14)$$

where the two leading terms, i.e. $(1+f_{21})(1-f_{w2})$, represent the effect of wall-proximity and f_{22} denotes the effect of free-turbulence [5]. The model functions f_{21}, f_{w2} are obtained by fitting the DNS data [6], which satisfy the limiting behavior of the wall:

$$f_{21} = \exp(-2\times 10^{-4}R^{13})(1-\exp(-2.2R^{0.5})) \quad (15)$$

$$f_{w2} = \exp(-5.5\times 10^{-2}R_y - 5.0\times 10^{-5}R_y^3 - 7.0\times 10^{-9}R_y^5). \quad (16)$$

As seen in equation (15), f_{21} is a function of the shear parameter R, which is defined as

$$R = \left(\frac{Sk}{\varepsilon}\right)\frac{f_{w2}}{R_t^{1/2}} \quad (17)$$

where R was derived from the scaling argument [19]. The effect of free-turbulence is also taken into consideration in the function f_{22},

$$f_{22} = 1-0.3\exp(-(R_t/6.5)^2) \quad (18)$$

which is obtained by curve-fitting the experimental results of grid-turbulence [20].

In the standard k–ε model, the production term P_ε^3 is generally neglected. However, the DNS data near the wall reveals that P_ε^3 is comparable to the turbulent diffusion term in the ε-budget, and, therefore, it is needed to balance the exact near-wall behavior of k and ε. Rodi and Mansour [19] derived the following model terms by manipulating the Navier–Stokes equations,

$$P_\varepsilon^3 = C_1\nu\nu_t U_{,jj}^2 + C_2\nu\left(\frac{k}{\varepsilon}\right)k_{,j}U_{,j}U_{,jj} \quad (19)$$

where $C_1 = 1.0$, $C_2 = 0.006$. On the basis of this model, a slightly modified model is introduced in the present study by utilizing the wall-reflection function f_{w1}. This approach ensures that P_ε^3 be located within the wall layer ($y^+ \leqslant 30$).

$$P_\varepsilon^3 = (C_1\nu\nu_t S_{,j}^{*2} + C_2\nu\left(\frac{k}{\varepsilon}\right)k_{,j}S^*S_{,j}^*)f_{w1} \quad (20)$$

where S^* is a modified strain rate parameter. The model constants C_1 and C_2 are set as $C_1 = 1.0$, $C_2 = 0.006$, respectively. As can be seen in equation (20), the first derivative of mean velocity is replaced with a simplified mean strain rate S^*. In the vicinity of the wall, the mean strain rate parameter S is affected mainly by the term $\partial U/\partial y$,

$$S^* = \frac{\partial U}{\partial y} = \frac{\tau_w/\rho}{\nu+\nu_t} = \frac{u_\tau^2}{\nu+\nu_t}. \tag{21}$$

By using the Kolmogorov scales, $\eta = (\nu^3/\varepsilon)^{1/4}$, $v = (\nu\varepsilon)^{1/4}$, we obtain the following formulation in concert with the relations $v\eta/v = 1$ and $\varepsilon^+ = \nu\varepsilon/u_\tau^4$,

$$u_\tau = \left(\frac{1}{\varepsilon^+}\right)^{1/4} v. \tag{22}$$

Consequently, S^* has a simplified form,

$$S^* = C_\tau \frac{\sqrt{(\nu\varepsilon)}}{\nu+\nu_t}. \tag{23}$$

Here, it can be seen that the model constant C_τ is replaced by the term $1/\sqrt{\varepsilon^+}$. The DNS data [6] reveals that the influence of $1/\sqrt{\varepsilon^+}$ on S^* within the wall layer ($y^+ \leqslant 30$) is shown to be negligible. Thus, C_τ is set as $C_\tau = 2.75$. It is recalled that S^* is used in the P_ε^3 model (f_{w1}). By choosing S^* instead of equation (19), it shows that the near-wall behavior in separated and reattaching flows can be resolved with a good accuracy.

The summarized form of ε-equation, which is used in the present study, is expressed in the following:

$$U_j\frac{\partial\varepsilon}{\partial x_j} = \frac{\partial}{\partial x_j}\left[\left(\nu+f_\varepsilon\frac{\nu_t}{\sigma_\varepsilon}\right)\frac{\partial\varepsilon}{\partial x_j}\right] + 1.45(0.95+0.05P_k/\varepsilon)P_k\frac{\varepsilon}{k} - 1.9f_2\frac{\varepsilon^2}{k} + \left(\nu\nu_t S_{,j}^{*2} + 0.006\nu\left(\frac{k}{\varepsilon}\right)k_{,j}S^*S_{,j}^*\right)f_{w1}. \tag{24}$$

3. NONLINEAR k–ε MODEL FOR REYNOLDS-STRESS TENSOR

As is well understood, the standard k–ε models have some critical deficiencies [10]. One major deficiency is the inability of the model to properly predict the effects of Reynolds stress relaxation. Another deficiency is that the model is oblivious to the presence of rotational strains in turbulent flows. In a recirculating flow past a backward-facing step, for example, the principal axes of Reynolds stresses are not always aligned with those of mean strain rates. In an effort to alleviate these shortcomings, a nonlinear or anisotropic generalization of eddy viscosity models has been vigorously pursued [10]. Details regarding the literature survey and relevant models can be found in the review paper of Speziale [10].

Speziale constructed a nonlinear k–ε model with the second-order term and this model was tested to the flow past a backward-facing step [10]. Horiuti examined the roles of higher-order terms, i.e. the third-order term in the nonlinear model, and he discussed the relationship with the algebraic stress model [21]. Recently, Craft *et al.* [22] put forward a third-order anisotropic representation for Reynolds stresses, and the model was applied to impinging jets. In the present study, the roles of third-order term have been scrutinized, however, the relatively small effects of the third-order term are estimated. Computations were made for the flow behind a backward-facing step, and the results indicate that the nonlinear model up to the second-order expression depicts the dominant flow structures satisfactorily. The Reynolds stresses up to the second-order expansion, which were employed in the present study, are

$$\overline{u_iu_j} = \tfrac{2}{3}k\delta_{ij} - 2\nu_tS_{ij} + 0.6\nu_t\frac{k}{\varepsilon}(S_{im}S_{mj} - \tfrac{1}{3}S_{mn}S_{mn}\delta_{ij}) + 0.4\nu_t\frac{k}{\varepsilon}(\omega_{im}S_{mj} + \omega_{jm}S_{mi}) + 0.005\nu_t\frac{k}{\varepsilon}(\omega_{im}\omega_{jm} - \tfrac{1}{3}\omega_{mn}\omega_{mn}\delta_{ij}). \tag{25}$$

In the above, the model constants were determined by using the experimental results [23].

4. APPLICATION TO ATTACHED BOUNDARY LAYER FLOWS

The thrust of the present model is to predict a separated and reattaching flow without using y^+. However, it is important to ascertain the generality and accuracy of the present model to an attached boundary layer. Toward this end, we have applied the model to a fully-developed channel flow, for which turbulence quantities are available from the DNS data [6].

The profiles of mean velocity, turbulent kinetic energy and its dissipation rate are exhibited in Figs. 1–3, respectively. The selected Reynolds numbers are

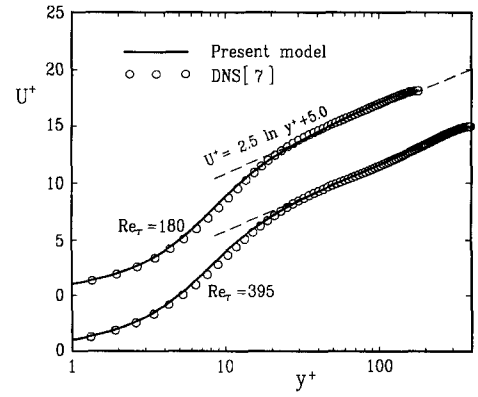

Fig. 1. Comparison of the predicted U with DNS in channel flow (Re_τ = 180 and 395).

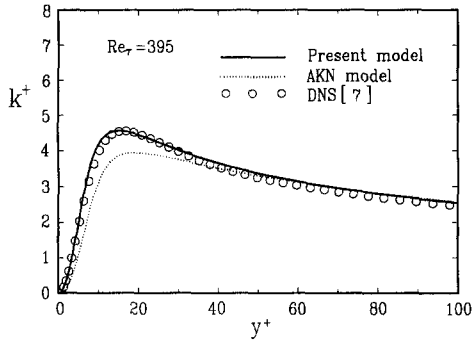

Fig. 2. Comparison of the predicted k in the near-wall region ($Re_\tau = 395$).

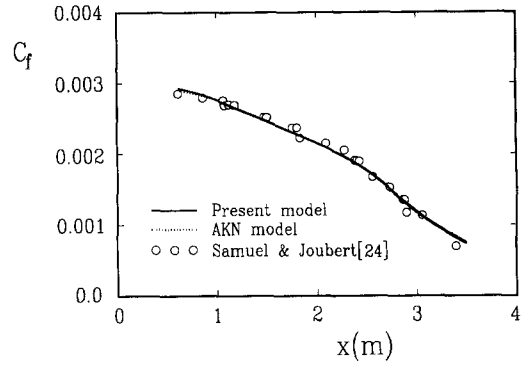

Fig. 4. Comparison of the predicted C_f in a strong adverse pressure gradient flow.

$Re_\tau = 180$ and $Re_\tau = 395$, for which DNS data exist. For mean velocity, the present model results are in good agreement with the DNS data in Fig. 1. The profiles of turbulent kinetic energy k^+ are shown in Fig. 2, in which the present model is seen to be in excellent agreement with the DNS data. As addressed in the Introduction, the model of Abe, Kondoh and Nagano [8] (hereafter referred to as AKN model) used the Kolmogorov velocity scale instead of the friction velocity (u_τ) to account for a separated and reattaching flow. In order to verify our model, the AKN model is adopted for comparisons. This is based on the belief that the AKN model is recently developed and can be regarded as a reliable model for predicting turbulent separated and reattaching flows. As shown in Fig. 2, the AKN model slightly underpredicts over the region $y^+ \leqslant 30$. This may be attributed to the overprediction of ε in this region. The near-wall behavior of ε is displayed in Fig. 3. The ε^+ profiles of AKN model overpredict in the region $y^+ \leqslant 30$. However, the present model results follow the DNS data fairly well. Furthermore, the maximum value of ε^+ very close to the wall is clearly displayed.

As stressed in Nagano and Tagawa [5], the existing k–ε models do not predict satisfactorily with adverse pressure gradient. Accurate prediction of an adverse pressure gradient flow is crucial, in particular, in analyzing complex turbulent flows. In an effort to assess the capability of the present model, the strong adverse pressure gradient flow is adopted for testing. The predicted result for C_f is shown in Fig. 4, compared with the prediction of the AKN model and the experiment of Samuel and Joubert [24]. Obviously, the present prediction is in excellent agreement with the experimental data.

Based on the reliable present model, the thermal field in a fully developed flow with a uniform wall temperature is calculated in Fig. 5, where the relevant DNS data is also available [25]. To analyze the turbulent heat transfer, the eddy diffusivity for heat is used together with the most probable turbulent Prandtl number concept, i.e. $Pr_t = 1.0$. The predicted results are compared with the computed data of AKN model [8] and the DNS data [25]. As seen in Fig. 5, the present model gives satisfactory results.

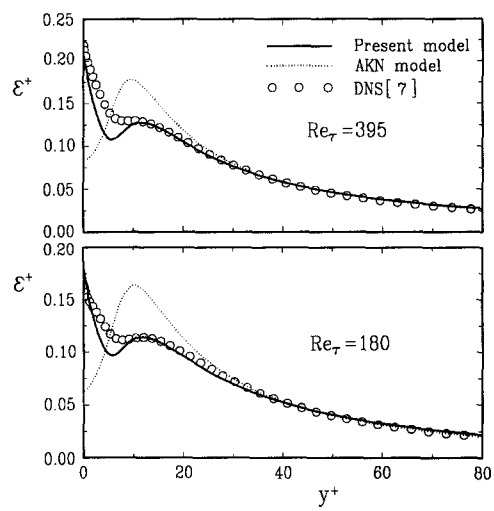

Fig. 3. Comparison of the predicted ε in the near-wall region ($Re_\tau = 180$ and 395).

5. APPLICATION TO BACKWARD-FACING STEP FLOWS

5.1. *Numerical procedure*

The finite-difference equations are discretized using the hybrid linear and parabolic approximation

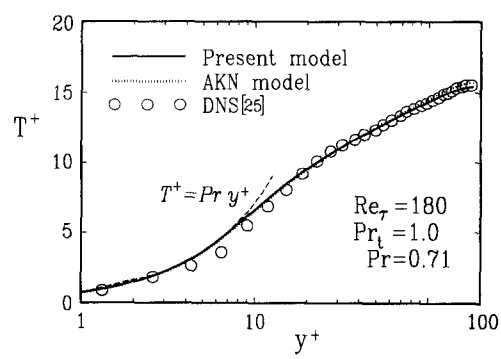

Fig. 5. Comparison of the predicted T with DNS in channel flow ($Re_\tau = 180$).

(HLPA) scheme with second-order accuracy. A non-staggered variable arrangement is adopted with the momentum interpolation technique to avoid the pressure-velocity decoupling. The coupling between pressure and velocity is achieved by the SIMPLEC predictor-corrector algorithm, which is an improved version of the SIMPLE algorithm. The set of discretized linear algebraic equations is solved by a strongly implicit procedure (SIP) [26].

The inlet and outlet of the computational domain of the backward-step flow are located $5H$ upstream and $30H$ downstream of the separation point, respectively. Here, H represents the step height. The inlet conditions are given from the experimental conditions. For comparison purposes, several test cases are summarized in Table 1. The no-slip boundary conditions are employed at the walls: $U = V = k = 0, \varepsilon_w = \nu\partial^2 k/\partial y^2, T = T_w$ and $\partial p/\partial y = 0$. The Neumann conditions are applied at the outlet.

The computations were implemented on a CRAY-YMP supercomputer, and a typical CPU time was approximately 3 h for one set of calculations. Convergence was declared when the maximum normalized sum of absolute residual sources over all the computational nodes was less than 10^{-4}. Several trial calculations were repeated to monitor the sensitivity of the results to grid size. The non-orthogonal finer-resolution grid systems were adopted, where the grid points were crowded near the wall boundaries and clustered in the recirculating region. The grid convergence was checked, the outcome of these tests was found to be satisfactory (201×121).

5.2. *Results and discussion*

All the computations of the backward-facing step flow are performed with the non-orthogonal grid system. Table 1 lists the conditions for the experiments on the backward-facing step flow [11–15]. Especially, the direct numerical simulation of turbulent flow over a backward-facing step by Le *et al.* [7] is of interest, in which the step-height Reynolds number is relatively low ($Re_H = 5100$).

First, the effect of non-equilibrium of the present model is considered. This effect is represented in the damping function of eddy viscosity ($f_\mu = f_{\mu 1} f_{\mu 2}$) and in the model constant $C^*_{\varepsilon 1} = C_{\varepsilon 1}(0.95 + 0.05 P_k/\varepsilon)$ in the ε-equation. The calculations are carried out for the eddy viscosity (ν_t) and the results are displayed in

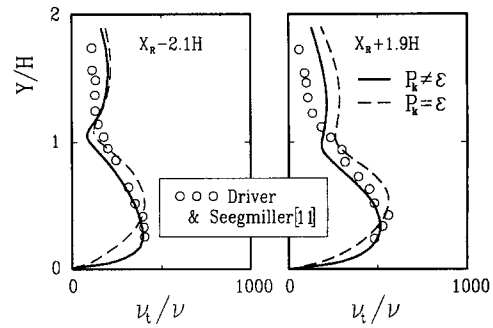

Fig. 6. Comparison of the predicted ν_t with experiment.

Fig. 6 for the recirculating region ($X_R - 2.1H$) as well as for the relaxing region ($X_R + 1.9H$). The dashed line represents the model of local-equilibrium state, i.e. $f_\mu = f_{\mu 1}$ and $P_k = \varepsilon$. Comparisons are made with the experimental data of Driver and Seegmiller [11] for $Re_H = 38\,000$. It is encouraging that the present results are in broad agreement with the experimental data. The agreement is better in the recirculating flow region rather than in the recovery region. This appears to be a common feature of other reattaching flow calculations [27, 28].

Comparisons are extended to the distributions of the turbulent kinetic energy (k/U_0^2) and the corresponding Reynolds stress ($-\overline{uv}/U_0^2$), as shown in Fig. 7. The predicted results of the turbulent energy by the two models agree reasonably well with the experimental data except in the upper recirculating region. A closer inspection of the distributions in the recirculating region indicates that the present model prediction ($P_k \neq \varepsilon$) is in better agreement with the experiment than the case of the local equilibrium model ($P_k = \varepsilon$). As for the Reynolds stress, the computational results of the non-equilibrium model are more consistent with the experimental data, especially in the recirculating region. These comparisons reinforce the capability of the present non-equilibrium model for predicting the recirculating flows over a backward-facing step.

The second step is to investigate the nonlinear representation for Reynolds stresses, as in equation (25). For comparison, the linear model of Abe *et al.* (AKN model) is also employed. Calculations are carried out for the flow over a backward-facing step ($Re_H = 5100$) and analyses are made with the DNS data of Le *et*

Table 1. Computational conditions for backward-facing step flows

Case	ER	Re_H	Re_θ	δ_s/H	Grid (non-orthogonal)
Driver and Seegmiller[11]	1.125	38 000	5000	1.5	201×121
Adams and Johnston[12]	1.25	36 000	3700	1.0	201×121
Kim *et al.*[13]	1.50	46 000	1500	0.25	201×121
Eaton and Johnston[14]	1.667	38 000	1000	0.23	201×121
Vogel and Eaton[15]	1.25	28 000	3370	1.1	201×121
DNS[7]	1.20	5100	667	1.1	201×121

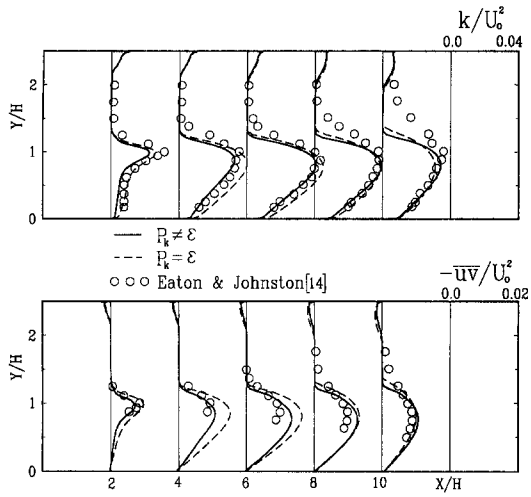

Fig. 7. Comparison of the predicted k/U_0^2 and $-\overline{uv}/U_0^2$ with experiment.

al. [7], as shown in Fig. 8. It is interesting that the predictions of U/U_0 and $-\overline{uv}/U_0^2$ by the two models are similar, but noticeable differences are found in the streamwise velocity fluctuations, $\sqrt{u^2}/U_0$. As can be seen in Fig. 8, the AKN model gives slightly lower values than the DNS data. This discrepancy is thought to be attributable to the isotropic assumption of the AKN model, which is also addressed by Abe *et al.* [8]. Although the present model is not entirely consistent with the DNS data, the present nonlinear model results are in better overall agreement well the DNS data in the recirculating region than the linear model.

Further evidence of the present model performance

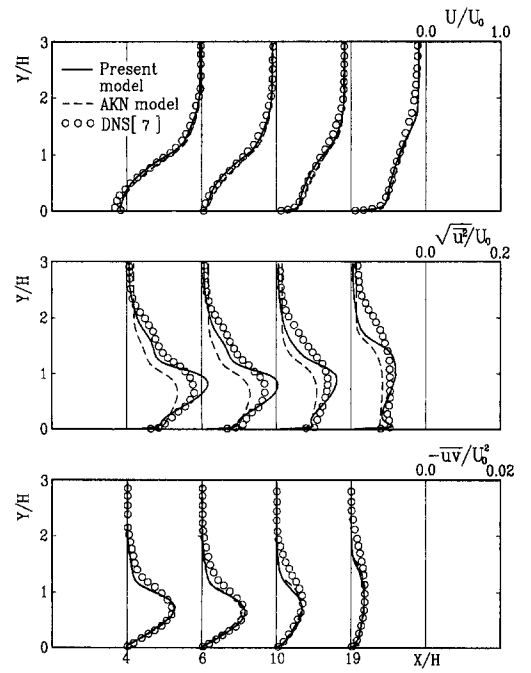

Fig. 8. Comparison of the predicted U/U_0, $\sqrt{u^2}/U_0$ and $-\overline{uv}/U_0^2$ with DNS.

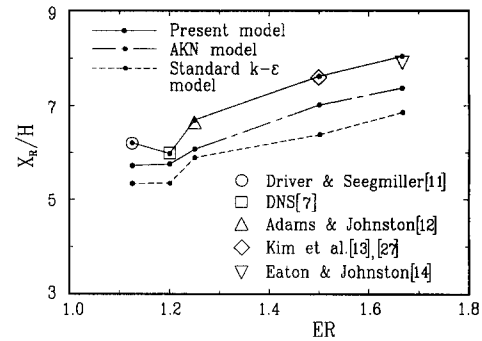

Fig. 9. Comparison of the predicted X_R with experiment.

is seen in the comparison of the calculated reattachment lengths, X_R/H, with the experimental results. As in Fig. 9, the present computational results are in excellent agreement with the experiments. Furthermore, the agreement is widely distributed to the ranges, where the adopted experimental conditions cover the far-ranges, $5100 \leqslant Re_H \leqslant 46\,000$ and $1.125 \leqslant ER \leqslant 1.667$. Here ER denotes the expansion ratio. The reattachment lengths by the standard k–ε model are seen to be underpredicted. It is also observed that, at least in the present computations by utilizing our numerical code, the AKN model predicts slightly lower values of reattachment length.

For the prediction of turbulent heat transfer near the wall-region of separated and reattaching flows, accurate calculations of eddy viscosity are indispensable [1, 8]. Since the majority of the heat transfer resistance occurs in the near-wall region, the level of skin friction is crucial to the prediction of heat transfer. The computed wall shear stress coefficient C_f against a nondimensional streamwise coordinate $X^* = (X - X_R)/X_R$ is shown in Fig. 10, together with the measurements of Eaton and Johnston [14]. It is seen that the present non-equilibrium model prediction in the recirculation region is in good agreement

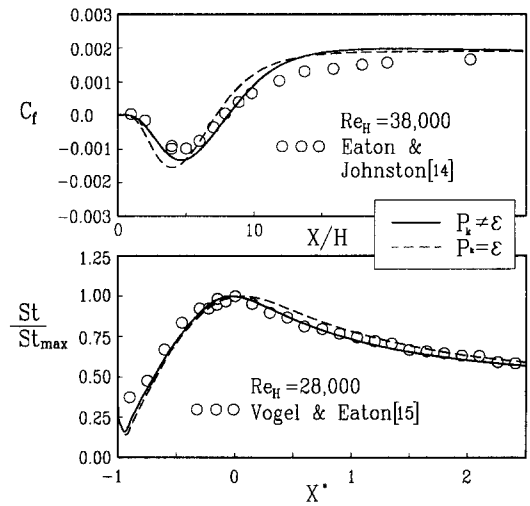

Fig. 10. Comparison of the predicted C_f and St/St_{max} with experiment.

with the experiment. This implies that the present model captures well the strong inhomogeneous flows in the recirculating region. The normalized Stanton number St/St_{max} is plotted in Fig. 10 with the experimental data of Vogel and Eaton [15]. The step-height Reynolds number is $Re_H = 28\,000$ and the heat flux through the heat transfer surface is 270 W m^{-3}. Other experimental conditions are listed in Table 1. The computed and experimental data show the same general features, i.e. the peak heat transfer rate occurs slightly upstream of reattachment ($X^* = 0$) and there is a low heat transfer rate in the recirculation region. It is seen that the present non-equilibrium model ($P_k \neq \varepsilon$) is in better agreement with the experiment than the model of the local equilibrium model ($P_k = \varepsilon$).

The streamwise variations of the local maximum of the streamwise turbulent intensity $(\overline{u^2}/U_0^2)_{max}$ and the Reynolds shear stress $(-\overline{uv}/U_0^2)_{max}$ are compared with the experiment of Eaton and Johnston [14] in Fig. 11. The computed results by two models are qualitatively consistent with the experiment. The measurements are located between the two calculated curves. It is believed that this discrepancy is due to the nonlinear representation for the Reynolds stresses. Regarding the Reynolds stress, the computational results by the two models show slightly higher values, particularly in the region around and upstream of the reattachment point.

6. CONCLUSION

An improved version of nonlinear low-Reynolds-number k–ε model has been developed for which allows the calculation of turbulent separated and reattaching flows with heat transfer. The main emphasis was placed on the usage of R_y ($\equiv k^{1/2}y/\nu$) instead of y^+ ($\equiv u_\tau y/\nu$) in the low-Reynolds-number model. The effects of low-Reynolds near the wall and the non-equilibrium effect in the recirculating region away from the wall were fully incorporated together with the wall limiting behavior of the ε-equation. In the first, the present model was tested against the DNS data of a fully developed channel flow. The predicted results for k and ε reproduced the correct wall limiting behaviors of flow fields quite successfully. Furthermore, the present model predicted the strong adverse pressure gradient flow satisfactorily. The validation was extended to the flows behind a backward-facing step. The effect of non-equilibrium ($P_k \neq \varepsilon$) was verified for calculating the eddy viscosity (ν_t), turbulent energy (k) and Reynolds stress ($-\overline{uv}$). The predicted results with the present non-equilibrium model were shown to be better agreement with the experiments rather than the local equilibrium model ($P_k = \varepsilon$). The nonlinear model up to second-order expansion was also examined and the predicted streamwise velocity fluctuations ($\overline{u^2}$) were consistent with the experiment satisfactorily among others. In particular, the calculated flow reattachment length (X_R) showed excellent agreement with the experiments and the relevant DNS data. For the prediction of turbulent heat transfer near the wall-region of separated and reattaching flows, several flow features were calculated and compared with the experiment. They were found to be qualitatively consistent with the experiment.

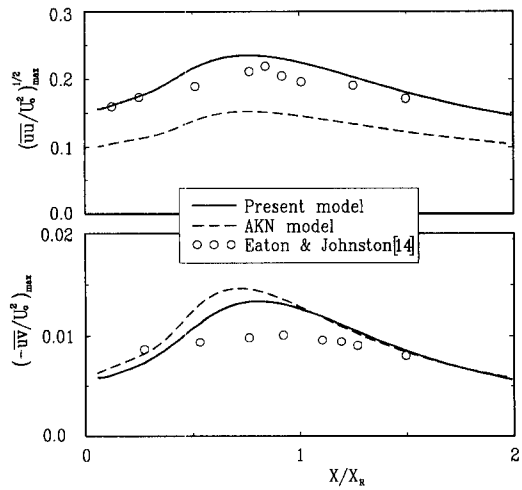

Fig. 11. Comparison of the predicted $(\overline{uu}/U_0^2)_{max}^{1/2}$ and $(-\overline{uv}/U_0^2)_{max}$ with experiment.

REFERENCES

1. B. E. Launder, On the computation of convective heat transfer in complex turbulent flows, *ASME J. Heat Transfer* **110,** 1112–1128 (1988).
2. C. L. Yap, Turbulent heat and momentum transfer in recirculating and impinging flows, Ph.D. Thesis, UMIST, Manchester (1987).
3. K. Suzuki, K. Suga, Y. Oshikawa and C. G. Lee, LDV measurement of turbulence and test of turbulence models in a recirculating flow, *Proceedings of the Sixth Symposium on Turbulent Shear Flows*, pp. 15.1–15.4, France (1987).
4. V. C. Patel, W. Rodi and G. Scheuerer, Turbulence models for near-wall and low Reynolds numbers flows: a review, *AIAA J.* **23,** 1308–1319 (1985).
5. Y. Nagano and M. Tagawa, An improved k–ε model for boundary layer flows, *J. Fluids Engng* **112,** 33–39 (1990).
6. N. N. Mansour, J. Kim and P. Moin, Reynolds-stress and dissipation rate budgets in a turbulent channel flow, *J. Fluid Mech.* **194,** 15–44 (1988).
7. H. Le, P. Moin and J. Kim, Direct numerical simulation of turbulent flow over a backward-facing step, *Proceedings of the Ninth Symposium on Turbulent Shear Flows*, pp. 13.2.1–13.2.5 (1993).
8. K. Abe, T. Kondoh and Y. Nagano, A new turbulence model for predicting fluid flow and heat transfer in separating and reattaching flows—I. Flow field calculations, *Int. J. Heat Mass Transfer* **37,** 139–151 (1994).
9. W. Rodi, The prediction of free boundary layers by use of a two-equation model of turbulence, Ph.D. Thesis, University of London (1972).
10. C. G. Speziale, Analytical methods for the development of Reynolds-stress closures in turbulence, *A. Rev. Fluid Mech.* **23,** 107–57 (1991).
11. D. M. Driver and H. L. Seegmiller, Features of a reattaching turbulent shear layer in divergent channel flow, *AIAA J.* **23,** 163–171 (1985).
12. E. W. Adams and J. P. Johnston, Flow structure in the

near-wall zone of a turbulent separated flow, *AIAA J.* **26,** 932–939 (1988).
13. J. Kim, S. J. Kline and J. P. Johnston, Investigation of a reattaching turbulent shear layer: flow over a backward-facing step, *J. Fluids Engng* **102,** 302–308 (1980).
14. J. K. Eaton and J. P. Johnston, A review of research on subsonic turbulent flow reattachment, *AIAA J.* **19,** 1093–1100 (1981).
15. J. C. Vogel and J. K. Eaton, Combined heat transfer and fluid dynamic measurements downstream of a backward-facing step, *ASME J. Heat Transfer* **107,** 922–929 (1985).
16. C. K. G. Lam and K. Bremhorst, A modified form of the k–ε model for predicting wall turbulence, *ASME J. Fluids Engng* **103,** 456–460 (1981).
17. C. Zhang, A. C. M. Sousa, Numerical simulation of turbulent shear flow in an isothermal heat exchanger model, *ASME J. Fluids Engng* **112,** 48–55 (1990).
18. N. Nagano and M. Shimada, Modeling the dissipation-rate equation for two-equation turbulence model, *Proceedings of the Ninth Symposium on Turbulent Shear Flows*, pp. 23.2.1–23.2.6, Japan (1993).
19. W. Rodi and N. N. Mansour, Low Reynolds number k–ε modelling with the aid of direct simulation data, *J. Fluid Mech.* **250,** 509–529 (1993).
20. G. K. Batchelor and A. A. Townsend, Decay of isotropic turbulence in the initial period, *Proc. R. Soc. Lond. A* **193,** 539–558 (1948).
21. K. Horiuti, Higher-order terms in the anisotropic representation of Reynolds stresses, *Phys. Fluid A* **2,** 1708–1710 (1990).
22. T. J. Craft, B. E. Launder and K. Suga, Extending the applicability of eddy viscosity models through the use of deformation invariants and non-linear elements, *Proceedings of the Fifth International Symposium on Refined Flow Modelling and Turbulence Measurements*, Paris (1993).
23. F. M. Champagne, V. G. Harris and S. Corrsin, Experiments on nearly homogeneous turbulent shear flow, *J. Fluid Mech.* **41,** 81–139 (1970).
24. A. E. Samuel and P. N. Joubert, A boundary layer developing in an increasingly adverse pressure gradient, *J. Fluid Mech.* **66,** 481–505 (1974).
25. J. Kim and P. Moin, Transport of passive scalars in a turbulent channel flow. In *Turbulent Shear Flows* (Edited by J. C. Andre *et al.*), Vol. 6, pp. 85–96. Springer, Berlin (1989).
26. S. Majumdar, Development of a finite-volume procedure for prediction of fluid flow problems with complex irregular boundaries, Report SFB 210/T/29, University Karlsruhe (1986).
27. R. K. Avva, S. J. Kline and J. H. Ferziger, Computation of the turbulent flow over a backward-facing step using the zonal modeling approach, Rep. No. TF-33, Stanford University, Stanford, CA (1988).
28. R. M. C. So, Y. G. Lai and G. J. Yoo, Low-Reynolds-number modelling of flows over a backward-facing step, *J. Appl. Math. Phys.* **39,** 13–27 (1988).